PRELIMINARY GN&C DESIGN FOR THE ON-ORBIT AUTONOMOUS ASSEMBLY OF NANOSATELLITE DEMONSTRATION MISSION

Jing Pei[*], Matt Walsh[†], Carlos Roithmayr[‡], Chris Karlgaard[§], Mason Peck,[¶] and Luke Murchison[‖]

Small spacecraft autonomous rendezvous and docking (ARD) is an essential technology for future space structure assembly missions. The On-orbit Autonomous Assembly of Nanosatellites (OAAN) team at NASA Langley Research Center (LaRC) intends to demonstrate the technology to autonomously dock two nanosatellites to form an integrated system. The team has developed a novel magnetic capture and latching mechanism that allows for docking of two CubeSats without precise sensors and actuators. The proposed magnetic docking hardware not only provides the means to latch the CubeSats, but it also significantly increases the likelihood of successful docking in the presence of relative attitude and position errors. The simplicity of the design allows it to be implemented on many CubeSat rendezvous missions. Prior to demonstrating the docking subsystem capabilities on orbit, the GN&C subsystem should have a robust design such that it is capable of bringing the CubeSats from an arbitrary initial separation distance of as many as a few thousand kilometers down to a few meters. The main OAAN Mission can be separated into the following phases: 1) Launch, checkout, and drift, 2) Far-Field Rendezvous or Drift Recovery, 3) Proximity Operations, 4) Docking. This paper discusses the preliminary GN&C design and simulation results for each phase of the mission.

INTRODUCTION

CubeSat activities have become an important goal in NASA's technology roadmap. The agency recognizes the value of CubeSats as a platform for technology demonstrations and science missions. Assembly of multiple CubeSats in space into large structures such as a space telescope or solar panels could be tremendously beneficial for the science and engineering communities. Several research groups[1–5] are currently tackling the challenges associated with autonomous rendezvous and docking of small scaled spacecraft on orbit. The On-orbit Autonomous Assembly of Nanosatellites (OAAN) team at NASA Langley was formed in response to the Announcement of Opportunity for the pilot Early Career Initiative from the Space Technology Exploration Directorate (STED) at NASA Headquarters. The idea is to use magnets to perform the alignment and docking of two CubeSats during the final phase of a docking maneuver that will make the docking process robust in the presence of system uncertainties. Current ground demonstration[6] is ongoing to verify the

[*]GN&C Lead, Vehicle Analysis Branch, NASA Langley Research Center, Hampton, Virginia, 23681.

[†]Graduate Student, Mechanical and Aerospace Engineering Department, Cornell University, Ithaca, New York, 14853.

[‡]Senior Aerospace Engineer, Vehicle Analysis Branch, NASA Langley Research Center, Hampton, Virginia, 23681.

[§]Senior Aerospace Engineer, Analytical Mechanics Associates, Hampton, Virginia, 23666.

[¶]Associate Professor, Mechanical and Aerospace Engineering Department, Cornell University, Ithaca, New York, 14853.

[‖]Project Manager, Structural and Thermal Systems Branch, NASA Langley Research Center, Hampton, Virginia, 23681.

key system functionalities within the constraints of the 3 Degrees of Freedom (DOF) (2 translation DOF, 1 rotation DOF) environment.

The long-term vision of the OAAN mission is to dock multiple CubeSats that reside in similar orbits but were sent up by multiple launch vehicles. However, from a simplicity and risk standpoint, it is decided that the concept of operation (CONOPS) for the initial space demonstration will consist of two 3U+ CubeSats. The CubeSats are most likely to be placed in a LEO (Low Earth Orbit) similar to that of the International Space Station (ISS) with a semi-major axis of 6775 km, eccentricity of 0.00012, and inclination of 51.64 degrees. Depending on the launch provider constraints, the CubeSats could be released from the PPOD (Poly Picosatellite Orbital Deployer) simultaneously or up to 10 minutes apart. The relative separation velocity is assumed to be within 1 m/s in any direction in the Clohessy-Wiltshire[7] frame (R-bar or cross-track, V-bar or along-track, H-bar or orbit normal). The objective of the GN&C algorithms is to rendezvous and dock the two CubeSats, while bearing in mind desirable characteristics such as: modularity, robustness, and autonomy (minimal intervention from the ground station). It should handle a wide range of initial separation conditions and allow for the mission planners on the ground to speed or slow down the mission timeline given the fuel budget onboard. Currently, it is assumed that the main mission (from deployment to docking) will take no longer than 4 months.

Figure 1 is a timeline of the five distinct phases of the mission. After launch and deployment, there is a 5-6 day checkout phase. During checkout, tests are performed to check the health of the CubeSats to make sure all systems including avionics, sensors, actuators, and radios are in proper condition. The Cubesats will continue to drift apart during this time due to the differences in the orbital elements. After checkout, the Attitude Determination and Control System (ADCS) on each CubeSat will be turned on to initiate the de-tumble process and to make sure the CubeSats achieve the desired orientations. The de-tumble and re-orientation phase is anticipated to take anywhere between 10-15 orbits. Once the CubeSats have achieved their desired orientations and establish communication with the ground station, the far-field (long-range) rendezvous or drift recovery phase begins.
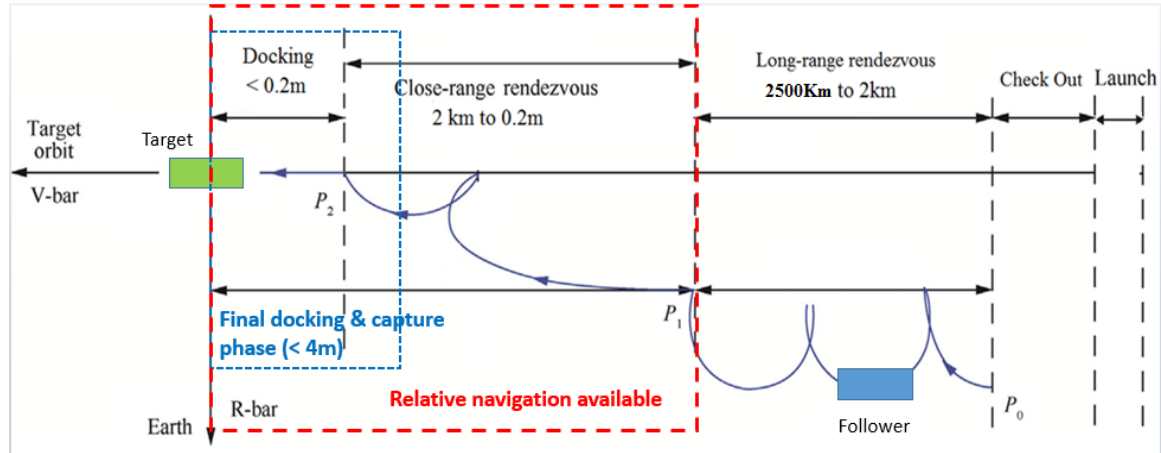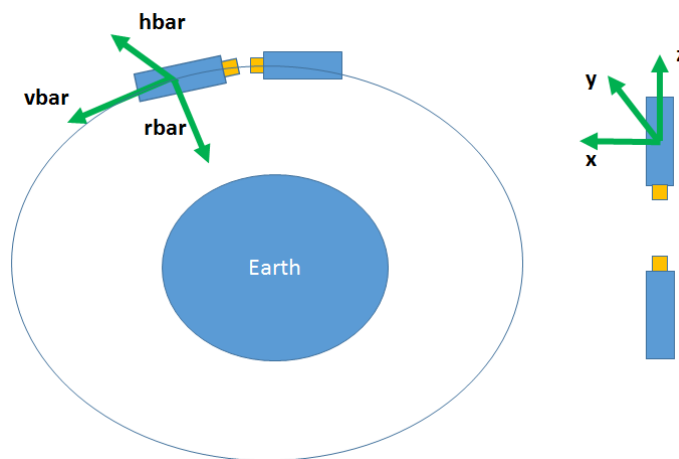

Figure 1. On Orbit Docking Concept of Operation

The far-field rendezvous or drift recovery phase is defined as the time during which the CubeSats do not have direct communication with each other and rely solely on the ground station for updates. Based on the specification for the radio, the threshold distance for relative position communication

is determined to be approximately 2 km. It is highly unlikely that the CubeSats will be within this distance after checkout. The lack of direct communication of relative state information requires the Follower CubeSat to communicate with the ground station first to obtain the states of the Leader CubeSat. The sequence of events in the drift recovery phase are as follows: 1) The Leader and Follower (Chief and Deputy) turn on their onboard GPS at the same epoch for 0.5 to 1 orbit to estimate the respective ECI (Earth Centered Inertial) position and velocity using GPS and onboard Extended Kalman Filter (EKF). 2) The CubeSats communicate their estimated states to the ground station through the RockBlock.[8] 3) The ground station uploads to the Follower the estimated mean differential orbital ephemeris and the Follower determines a desired ΔV (velocity increment) command. Alternatively, the ΔV computation could be done by the ground station and upload to the Follower. 4) Due to power constraints, once the ΔV command has been carried out by the Follower, both CubeSats turn off their GPS receivers and begin coasting. 5) Steps 1-4 are repeated until the Follower comes within 2 km of the Leader in the V-bar direction with minimal excess relative velocity and separation in the R-bar and H-bar directions. The drift recovery algorithm closely mimics that of the CanX 4 and 5 missions[9, 10] that successfully demonstrated rendezvous of two 3U Cube-Sats from more than 2000 km V-bar separation followed by precise formation flying. Following the proven CanX approach for the drift recovery phase significantly lowers the overall mission risks.

The proximity operations or close range rendezvous phase is defined as the time during which the CubeSats are within CDGPS (Carrier-Phase Differential Global Position System) radio range and the relative position states can be communicated back and forth continuously. Similar to the CanX formation flight mission, OAAN will utilize CDGPS[11] to determine the relative position of the two CubeSats by measuring the phase difference of the GPS carrier wave at two locations. It is proven that CDGPS can provide relative position measurement within a few centimeter accuracy. During the close-proximity operations phase, the Follower will perform high precision formation flying for 10 or so orbits. Upon successful completion, the Follower will be put on a catch-up trajectory such that it slowly maneuvers towards the Leader until the V-bar separation is less than 10 meters. A second series of formation flying experiments will be performed to verify the system performance prior to docking. Once that is successfully achieved, the ground station provides the Follower with approval for final docking. Figure 2 shows the adopted axis systems during the proximity operations and docking phases of the mission.

Figure 2. On-Orbit Docking Concept of Operation

3

During the docking phase, both the Leader and Follower will have their $\pm Z$ body axes directed along the local V-bar direction such that their docking interfaces are pointed towards each other. This operation is required because relative attitude information is assumed to be unavailable. The star tracker on both CubeSats is aligned with zenith for the best view of the stars. The translational controller will bring the Follower towards the Leader at a few cm/s. Once the CubeSats are within the basin of attraction[12] of the magnetic docking subsystem, feedback control on each CubeSat is turned off, allowing for passive elimination of residual relative position and attitude errors. The CubeSats will then align and complete the docking process.

It is worth noting that since the primary objective of the mission is to demonstrate the novel docking mechanism, the approach with the lowest risk would be to eject the CubeSats from the same PPOD deployer and separate them after they have been fully commissioned, similar to the CPOD mission.[1] Doing so would ensure that the CubeSats start out within CDGPS range and eliminate the need for a far-field rendezvous phase. This would significantly reduce the complexity and duration of the overall mission. However, there are not many launch providers that provide a 6U deployer, hence the far-field rendezvous phase is required to make the mission fully robust.

This paper is organized as into the following sections: The System Overview section provides an overview of the system dynamics. The Launch and Drift section describes the launch and check-out phase of the mission. The Drift Recovery section discusses the GN&C design of the far field rendezvous phase in which the CubeSats are outside of CDGPS range. Robustness of the GN&C design along with preliminary simulation results are shown. The Proximity Operations section addresses the proposed formation flying experiments. Finally, the Docking section describes the docking GN&C design and highlight the importance of the proposed magnetic docking mechanism for final docking.

SYSTEM OVERVIEW

Propulsion

For translational control, four cold gas thrusters are arranged such that they provide pure translational motion as shown in Fig 3. The thrusters are strategically placed at the corners of an imaginary tetrahedron (middle U of the 3U CubeSat) with the thrust vectors directed towards the centroid of the CubeSat. During the on-orbit operation, the center of mass (CM) is designed not to vary by more than 1 cm from the centroid. As a result, disturbance torque from the thrusters should be kept to a minimum. The estimated available ΔV is approximately 16 m/s. Detailed modeling of the propulsion subsystem performance is not included in the current simulation studies.

GPS/CDGPS

Due to size constraints, cost, and simplicity considerations, CDGPS was chosen as the relative navigation sensor, and only relative position measurements are available between the Leader and Follower CubeSat. Visual navigation methods, such as using lasers and cameras were out of the project scope. CDGPS[13,14] allows for a few cm relative positioning accuracy when a RTK (real time kinematic) solution or a "lock" has been achieved between two units, and it has been used successfully for precise CubeSat formation flight missions such as the CanX missions in 2014.[9] Therefore, in theory, the accuracy of the CDGPS should be adequate for a docking mission as well. The Swift Navigation Piksi[11] is the commercial CDGPS hardware solution that was selected for OAAN. The Piksi units require one external antenna that faces away from the Earth to point toward
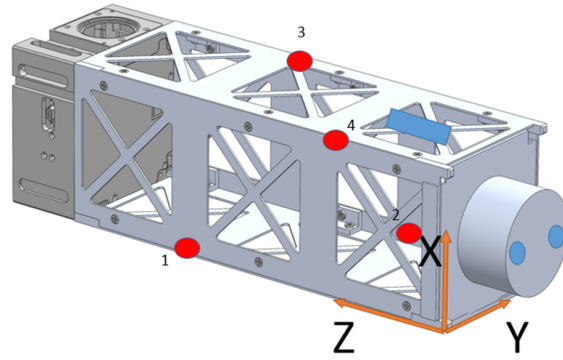
Figure 3. Thruster Layout

the GPS satellites. A pair of units is required to achieve a relative navigation solution. Once a RTK solution has been achieved between the two units, it will output a relative position and velocity vector between the two phase centers of the Piksi GPS antenna in the local North-East-Down (NED) or the Earth Centered Earth Fixed (ECEF) frame. In addition, the single-point (SPP) GPS solutions of the Piksi units will be used for absolute navigation during the far-field rendezvous phase when relative communication is not possible.

ADCS

The Attitude Determination and Control System (ADCS) is provided by Blue Canyon Technologies (BCT). The XACT[15] unit is a fully assembled commercial off-the-shelf product with flight heritage. The XACT provides precise three-axis attitude control using reaction wheels, magnetic torque rods, and integrated control algorithms. For attitude determination, it contains a star tracker, sun sensor, magnetometer, and on-board EKF. The star tracker is used during fine pointing mode operations. Note: simulation results presented in the paper are based on an assumption of perfect attitude determination and control.
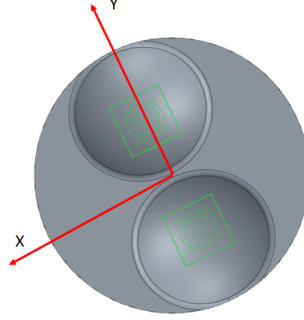
Magnetic Docking Subsystem

Considerations of simplicity and docking success would naturally lead one to use a single large permanent magnet for a docking subsystem. The magnetic docking mechanism makes the system more robust to residual relative errors in the attitude and position loops. Practical constraints such as volume, mass, and the impact a strong electromagnetic field on other subsystems provide a hard limit on the size of the magnet. From an attitude control perspective, a single magnetic dipole on board the CubeSat is problematic because a disturbance torque will be generated due to its interaction with the magnetic field of the Earth[16] shown in Eq. 1

$$\tau_d = M \times B \tag{1}$$

where M is the net magnetic dipole moment of the docking subsystem and B is the Earth's magnetic field. A 0.5 inch cuboid magnet would generate a disturbance torque that is greater than the available control torque from both the reaction wheels and the magnetic torque rods. Due to this constraint, the docking subsystem is required to have a nominal net dipole moment of zero. This requirement can be accomplished with a pair of magnets per docking subsystem with the dipoles having opposite

5

directions in the Z axis of the body frame. Figure 4 shows a schematic of the docking subsystem. The capture range associated with this design is smaller compared to the single dipole design due to the existence of unstable equilibrium conditions[12] in which the two docking subsystems would repel each other.

Figure 4. Magnetic Docking Subsystem Schematic

In addition to the zero net magnetic dipole requirement, the ADCS also requires that the magnetic docking subsystem shall not generate a changing magnetic field at the location of the magnetometer that is significant when compared to the geomagnetic field vector of the earth. For one degree of pointing accuracy, the magnetic field induced at the magnetometer location should be less than 0.7 μT. This further provides an upper bound on the strength of the magnetic dipoles. Equation 2 is used to estimate the magnetic field (B) induced at a certain distance (r) by a magnetic dipole moment of strength ($\vec{m}$).

$$B = \frac{\mu_o}{4\pi}\left[3\frac{(\vec{m}\cdot\hat{r})\hat{r} - \vec{m}}{|r|^3}\right] \tag{2}$$

Environment

Because the Earth is not symmetric and its mass is not uniformly distributed, a spherical harmonic model is typically used for the gravity field.[17] A zonal harmonic[18] gravity model was used to capture the effects of Earth's oblateness or bulge at the equatorial plane. The first seven zonal coefficients in the harmonic series are used in the simulation. They are shown in Table 1. Atmospheric drag is not modeled because the CubeSats are in very similar orbits and experience approximately the same aerodynamic effects. Hence, the differential aerodynamic forces are negligible. The same principle applies for solar radiation pressure. Gravity gradient torque is not included.

Table 1. Zonal Harmonic Gravity Terms

|	
J_2	$1.08263566655 \times 10^{-3}$
J_3	$-2.53247369133 \times 10^{-6}$
J_4	$-1.61997430578 \times 10^{-6}$
J_5	$-2.27905126082 \times 10^{-7}$
J_6	$5.40616789940 \times 10^{-7}$
J_7	$-3.50522925632 \times 10^{-7}$
J_8	$-2.04016767010 \times 10^{-7}$

6

LAUNCH AND DRIFT

The CubeSats are assumed to be deployed from the same launch vehicle at a typical 400 km altitude near-circular Low Earth Orbit (LEO). Table 2 shows the orbital elements associated with the ISS orbit. Right Ascension of the Ascending Node (RAAN), Ω, and Argument of Periapse, ω, are not shown in the table because they vary slowly over time due to J_2 effects.

Table 2. ISS Orbital Elements

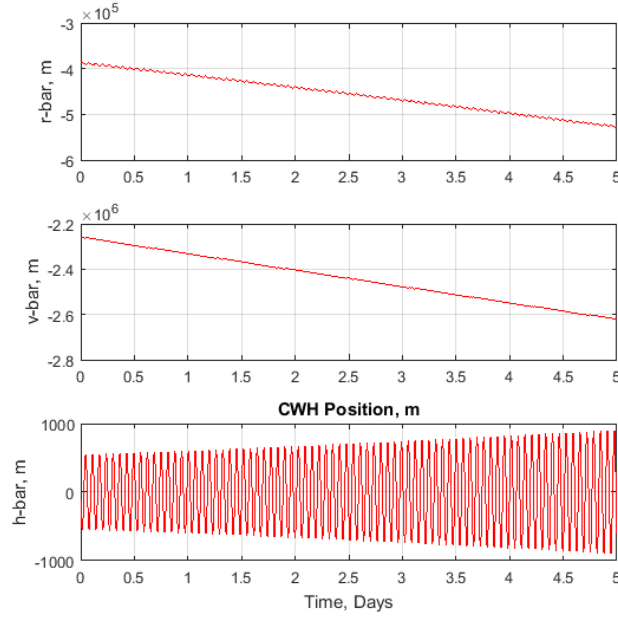| Orbital Elements	Values
Semi-major axis, a	6900 km
Inclination, i	51.64 deg
Eccentricity, e	0.0002

It is unlikely that a simultaneous separation of the CubeSats would take place as there are not many 6U+ PPOD deployers available to launch providers. With other factors in mind, there could be a 5 to 10 minute gap between separations. In addition, due to factors such as launch vehicle orientation or release mechanisms, etc. there will be some initial relative velocity between the CubeSats. It is well known from the classic Clohessy-Wiltshire (CW) equations that relative velocities in the R-bar or H-bar would result in oscillations about zero in the respective directions. However, relative velocities in the V-bar direction will cause a secular drift in the along-track direction. Generally, the checkout period for a CubeSat is around 5 to 6 days before it is considered fully commissioned. Depending on the initial relative velocity in the V-bar direction, after the commission period the CubeSats could be separated by thousands of kilometers. In the case of the CanX-4 and 5 mission,[9,10] the relative separation distance grew to 2300 km from deployment to the initiation of the drift recovery phase.
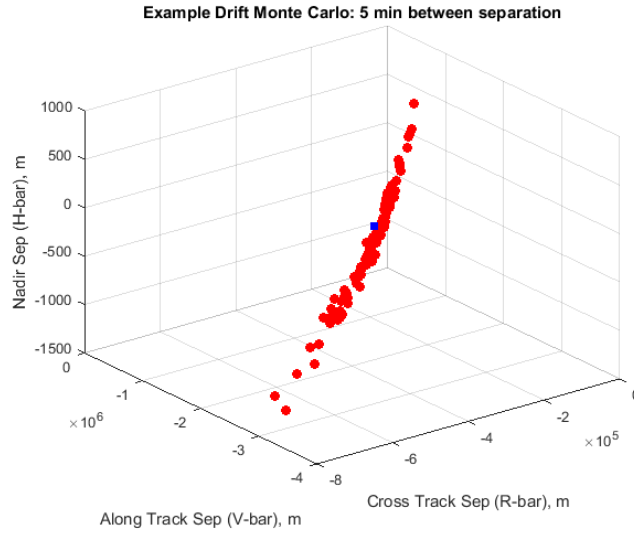
Figure 5. Example Drift Monte Carlo Results: ΔT = 5 min

Monte Carlo simulations were performed to obtain an approximate bound for the range of initial conditions at the beginning of the drift recovery phase. Figure 5 shows the results from one such

Monte Carlo run. Here the gap in the separation time was assumed to be 5 minutes (equivalent to some initial differences in true anomaly $\Delta\nu$) and the relative separation velocity was dispersed between 0 to 1 m/s in any direction. Depending on the relative V-bar velocity at the separation, the final CW distances could either grow or shrink over the 5 to 6 day drift period. Figure 6 is a plot of the relative distances in the CW frame for one of the more extreme cases in which the separation gap is 5 minutes and the relative separation velocity is -0.3 m/s in the V-bar direction.

Figure 6. Initial Drift Example: Relative Position CW frame

In this case, at the end of the 5-day checkout period, the CubeSats will be separated by over 2600 km and continue to drift apart due to differences in the orbital elements. Table 3 shows the mean differential orbital elements at the end of the checkout period.

Table 3. Example: Differential Mean Orbital Elements after 5 Day Checkout

Differential Orbital Elements	Values
Semi-major axis, Δa	-530 m
Inclination, Δi	-4.315×10^{-6} deg
Eccentricity, Δe	0.000038
Longtitude of the Ascending Node, $\Delta\Omega$	-0.023856 deg

DRIFT RECOVERY

The objective of the far-field rendezvous or drift-recovery phase is to move the Follower CubeSat from outside of CDGPS range given some initial conditions from the end of the checkout phase to inside CDGPS range, where it is directly behind the Leader in the CW frame. The cost function is to minimize any residual out-of-plane motion (R-bar and H-bar) as the Follower slowly approaches the

8

2-km threshold distance in the V-bar direction while simultaneously minimizing the ΔV consumption. In terms of mean orbital elements, at the beginning of the drift recovery phase the CubeSats are drifting apart due to differences in their orbital elements, and at the end of the phase the CubeSats should have nearly identical orbital elements except for a small difference in the true anomaly, ν.

The algorithm for the drift recovery phase closely mimics that used for the CanX-4 and CanX-5 formation flying mission which takes advantage of the natural orbital perturbations to conserve ΔV. A more detailed description of the CanX mission and a full derivation of the method can be found in Ref. [9, 10]. The drift recovery phase can be further broken into three distinct sub-phases. The objectives of Sub-phase 1 is to eliminate any initial drift rates and put the Follower on a desired return trajectory. The mission designer can specify a desired catch-up rate in the along-track direction by controlling the drift rate of the relative argument of latitude, $\delta\dot{\lambda}$, while simultaneously matching the Ω of the two orbits in the out-of-plane direction. Equation 3 is a first order Taylor Series expansion of $\delta\dot{\lambda}$ with respect to each relative orbital elements (semi-major axis, eccentricity, and inclination). The eccentricity and inclination terms both have negligible impacts on the catchup rate, thus only semi-major axis is use to adjust $\delta\dot{\lambda}$.

$$\dot{\lambda} = \left.\frac{\partial\delta\dot{\lambda}}{\partial a}\right|_{x_l} \delta a + \left.\frac{\partial\delta\dot{\lambda}}{\partial e}\right|_{x_l} \delta e + \left.\frac{\partial\delta\dot{\lambda}}{\partial i}\right|_{x_l} \delta i \tag{3}$$

Given the initial along-track separation in terms of $\delta\lambda$, the designer can specify a δa such that the Follower would get within some V-bar separation distance of the Leader given some desired time, T sec. In the out-of-plane direction, the precession in Ω between the two orbits due to J_2 must also be eliminated. This can be addressed by Eq. 4 and 5 in which the the designer can specify a target inclination for the Follower in order to match Ω with that of the Leader in T sec.

$$\dot{\Omega} = -\frac{3}{2}J_2\left(\frac{R_e}{a(1-e^2)}\right)^2\sqrt{\frac{\mu}{a^3}}\cos i_F \tag{4}$$

Here J_2 is the dominating zonal harmonic gravity term, R_e is the radius of the Earth, and μ is the universal gravitational constant. $\dot{\Omega}$ can be replaced as the finite difference between the Leader and Follower's Ω.

$$\dot{\Omega} = -\frac{\Omega_L - \Omega_F}{T} \tag{5}$$

Sub-phase 2 begins when the Follower is within some pre-determined V-bar separation distance from the Leader. Prior to reaching the 2-km V-bar target for close-proximity operations, the catchup rate must be reduced incrementally by specifying the desired Δa as a function of V-bar separation. This is referred to as the deceleration phase and significantly reduces the chance of the Follower overshooting the 2-km V-bar target distance. During this phase, groups of multiple thrusts could take place per orbit to eliminate any residual differences in e, ω, and i. Sub-phase 3 begins when the Follower is within approximately 15 km of the 2-km target distance with little out-of-plane motion. Here a Δa is specified such that the Follower slowly coasts toward the target at the rate of a few cm/s.

Throughout the entire drift recovery phase, the impulsive thrusts required to cause desired changes in the orbital elements can be computed based on the Gauss Variational Equations[19] (Eq. 6 to 10). Here ΔV_r, ΔV_t, and ΔV_z are the ΔV applied in the Follower's orbital radial, tangential, and normal directions respectively. The pseudo-inverse solution to these sets of equations provides the ΔV

required to achieve desired changes in the orbital elements.

$$\dot{a} = \frac{2a^2}{\sqrt{\mu a(1-e^2)}}[e \sin f \Delta V_r + \frac{p}{r}\Delta V_t] \tag{6}$$

$$\dot{e} = \sqrt{\frac{a(1-e^2)}{\mu}}[\sin f \Delta V_r + \frac{r(2\cos f + e(1+\cos^2 M))}{p}\Delta V_t] \tag{7}$$

$$\dot{i} = \sqrt{\frac{a(1-e^2)}{\mu}}\frac{r \cos \lambda}{p}\Delta V_z \tag{8}$$

$$\dot{\Omega} = \sqrt{\frac{a(1-e^2)}{\mu}}\frac{\sin \lambda}{p \sin i}\Delta V_z \tag{9}$$

$$\dot{\omega} = \sqrt{\frac{a(1-e^2)}{\mu}}\left[\frac{-\cos f}{e}\Delta V_r + \frac{r(2 + e\cos M)sinf}{pe}\Delta V_t - \frac{r \sin \lambda}{p \tan i}\Delta V_z\right] \tag{10}$$

Since OAAN is a low-cost and high-risk technology demonstration, the Piksi units onboard the CubeSats serve as the sole absolute and relative navigation sensors. When outside the 2-km range of the Piksi antennas, the Piksi single point solution (SPP) GPS data will be used by the EKF to estimate the CubeSat's absolute position and velocity in the ECI (Earth Centered Inertial) frame. Due to power constraints, the GPS and EKF on each CubeSat can only be turned on periodically to estimate the positional states. The estimated states will be sent to the ground station, transform to the orbital elements and pass through a FIR (Finite Impulse Response) filter to obtain an average. The mean differential orbital elements will be communicated back up to the Follower CubeSat. Table 4 compares the performance of the Piski in SPP mode vs. real time kinematic (RTK) mode. The SPP is the standalone, absolute GPS position solution using only a single receiver. The RTK solution is the differential GPS solution.[11] It is apparent that the RTK solution is roughly 2 orders of magnitude more accurate than SPP. However, the SSP solution should be adequate for the drift recovery phase where the objective is to get the Follower within 2 km of the Leader.

Table 4. Piksi: SPP vs. RTK

| Parameters	SPP	RTK
Number of Receivers	1 (Rover)	2 (Rover and Base)
Position Type	Absolute, ECEF	Relative
Position Accuracy (Horizontal)	3-5 meters	0.01 - 0.03 meters
Position Accuracy (Vertical)	12-15 meters	0.03 - 0.06 meters

In the preliminary implementation of the EKF,[20] the update rate of the filter is assumed to be 5 seconds. In between the epochs, a first-order Euler integration scheme (step size of 5×10^{-5} sec) is used to propagate the system dynamics. Due to the limited computational resources, a J_2 gravity model is used in the propagation of the orbital dynamics. This is deemed to be a good tradeoff between having a higher order model that captures the essential plant dynamics with computational efficiency. Details such as EKF initialization[14] and latencies associated with the periodic communications between the CubeSats with the ground station via RockBlock[8] are not included in the current analysis.

Typical measurement GPS covariance values are used in the preliminary EKF design. Both position and velocity measurements are assumed to be available. Equation 11 shows the measurement covariance matrix, R_d.

$$R_d = \text{diag}([\sigma_x^2 \ \sigma_y^2 \ \sigma_z^2 \ \Sigma_x^2 \ \Sigma_y^2 \ \Sigma_z^2]) \tag{11}$$

where σ is the GPS position covariance (10 m) and Σ is the GPS velocity covariance (0.125 m/s). The process noise covariance Q_d is assumed to be the RSS (root sum square) of the accelerometer covariance (0.002 m/s^2) with un-modeled dynamics, W (0.009 m/s^2). The un-modeled dynamics covariance, W accounts for the mismatch between the gravity model (J_2) inside the propagator and a high-fidelity gravity model (up to 300 coefficients).

Preliminary baseline results presented here are based on an assumption of perfect navigation measurements and actuators. The terminal conditions at the end of the checkout phase shown in Figure 6 and Table 3 are used as the initial conditions for the drift recovery simulation. Figure 7 shows the baseline return trajectory in terms of the absolute distance in the CW frame. After the checkout phase (Day 5), the Follower is placed on a slightly lower orbit (Δa) such that it arrests any initial drift rate and catches up to the Leader at a constant specified rate, $\delta\lambda$. Small corrections are applied during each estimation and firing interval to correct for any disturbances. During days 23 to 38, small amounts of ΔV are applied to correct for mean differences in e and ω. Day 39 marks the start of the deceleration sub-phase, in which the Follower gradually slows down incrementally prior to approaching the 2-km target location. During this sub-phase, small orbital matching burns were applied. The Follower reaches the 2-km V-bar target between Day 74 and 75. Figures 8 show plots of the relative position and velocity in the CW frame.
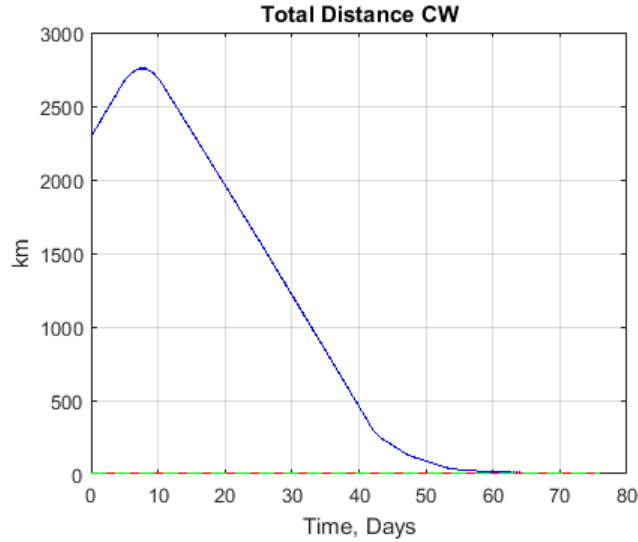
Figure 7. Drift Recovery Phase Example: Absolute Relative Position CW frame

Figure 9 shows the corresponding plots of the differential orbital elements. During the initial drift recovery phase, a desired inclination is specified for the Follower such that the difference in Ω is eliminated by the start of the deceleration sub-phase on Day 39. The adopted CanX algorithm appears to do a great job in slowly eliminating the differential orbital elements in a fuel efficient manner. The total ΔV consumed for this baseline drift recovery run is approximately 3 m/s. The designer could speed up the drift recovery phase by placing the Follower on an initial lower orbit at
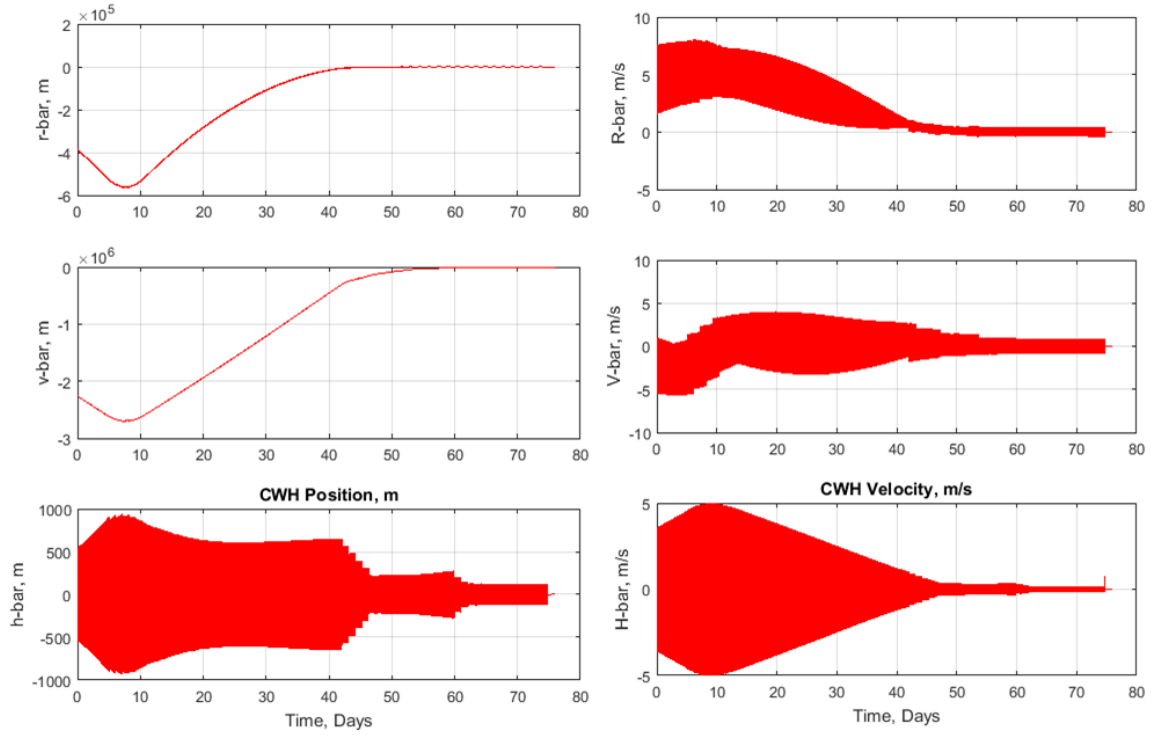
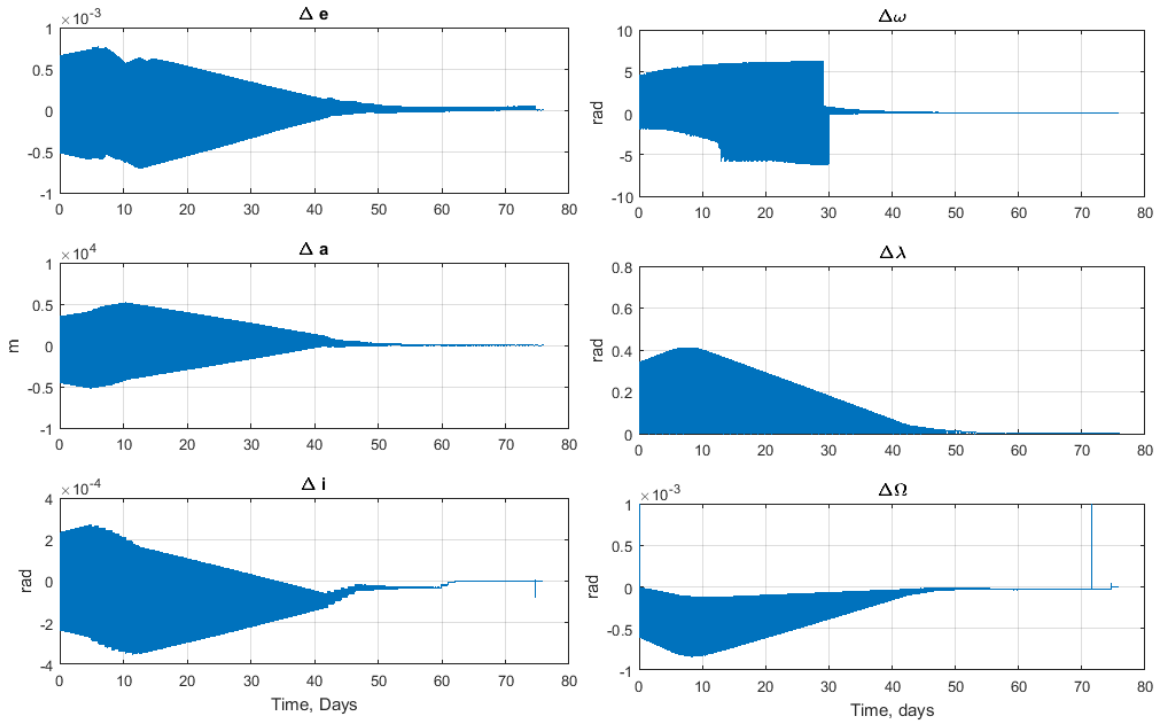**Figure 8. Drift Recovery Phase Example: Relative Position and Velocity CW frame**

the cost of additional ΔV.

Table 5 shows the final position and velocity states in the CW frame at the end of the baseline drift recovery phase. To access the robustness of the algorithm, a Monte Carlo simulation was performed in which the initial separation velocity between the CubeSats was dispersed (1 m/s in any direction) while assuming a 5 min separation gap. Figure 10 shows the final CW position and velocity along with the 3-sigma bound represented by the green contours. Even without any manual parameter tuning for each run, it is apparent that the baseline algorithm outlined above should be effective in bringing the Follower to a V-bar separation distance of 2 km behind the Leader with minimal residual out-of-plane velocities.
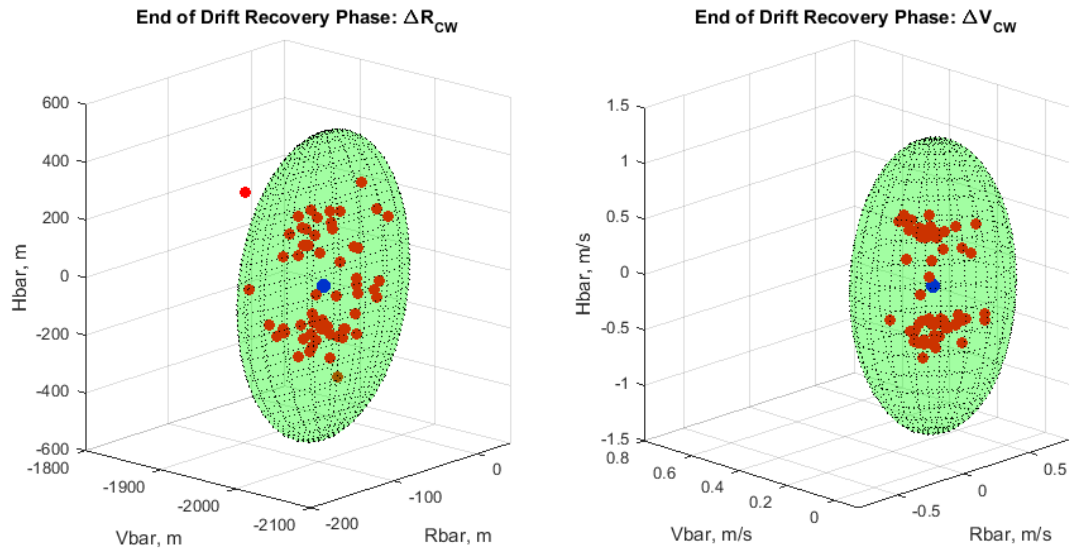
Table 5. Example: Final CW States at the end of Drift Recovery Phase

Parameters	Values		
Relative Position, m	$[-64$	-1996	$97]$
Relative Velocity, m/s	$[0.37$	0.17	$-0.07]$

Once the Follower CubeSat reaches the 2-km V-bar target location and establishes a RTK solution with the Leader's Piski. A full-state feedback controller can be used to eliminate any residual differences in the orbital elements. Table 6 shows the final differential orbital elements after the full-state feedback control has been applied. Note: full-state feedback continuous control is expensive from a ΔV consumption standpoint. It is imperative for the designer to tune the parameters in the drift recovery algorithm such that Follower reaches the 2-km target with minimal out-of-plane

Figure 9. Drift Recovery Phase Example: Differential Orbital Elements

Figure 10. Drift Recovery Monte Carlo: Final Relative Position and Velocity CW frame

errors.

Table 6. Example: Final Differential Orbital Elements at the end of Drift Recovery Phase

Differential Orbital Elements	Values
Semi-major axis, Δa	0 m
Inclination, Δi	1.1e-6 deg
Eccentricity, Δe	6×10^{-7}
Longitude of the Ascending Node, $\Delta\Omega$	1.1×10^{-5} deg
Argument of Perigee, $\Delta\omega$	1×10^{-4} deg
Argument of Latitude, $\Delta\lambda$	0.016971 deg

PROXIMITY OPERATIONS

The proximity operations or close-range rendezvous phase is defined as the time during which the CubeSats are within CDGPS range and the relative position states can be communicated back and forth without the ground station. The objective of the close-proximity operations phase is to have the Follower perform a series of initial high precision formation flights for approximately 10 orbits. This would allow the ground station to develop further confidence in the performance of the CDGPS, Navigation filters, and propulsion subsystem.

The formation-flying controller is a discrete LQR (Linear Quadratic Regulator) design about the CW equations shown in Eq. 12 to 14, where x, y, z are the relative separation distances in the R-bar, V-bar, and H-bar direction and ω is the frequency of the orbit. The proposed formation is a 2000 m along-track orbit, in which the Follower is commanded to stay perfectly behind the Leader at a standoff distance of 2000m with minimal variations in the cross-track and H-bar directions. The 2km distance offers a good buffer in case an off-nominal event occurs such as a loss of relative position communication. Another option would be to put the Follower on a passive walking safety ellipse[21] and perform nav-related tests during that period.

$$\ddot{x} = 3\omega^2 x + 2\omega\dot{y} \tag{12}$$

$$\ddot{y} = -2\omega\dot{x} \tag{13}$$

$$\ddot{z} = -\omega^2 z \tag{14}$$

Once the ground station deems the formation flight experiment successful, a small ΔV based on the Gauss Variational equations will be applied to the Follower such that it slowly catches up to the Leader at a few cm/s. Once the Follower is within 10 meters of the Leader in the V-bar direction, a second set of formation flying experiments is planned to re-assure the ground station about the performances of the sensors, actuators, and GN&C algorithms prior to final docking. Once the precise formation flying control is successfully demonstrated at a 10 m along track orbit, the docking command is given to the Follower. This is deemed to be the most risky portion of the mission as a loss of relative communication or similar failures would likely result in a collision between the two CubeSats.

Figure 11 shows the absolute relative distance in the CW frame for the sample case (magnified towards the end of the drift recovery phase shown in Fig. 7). Prior to day 78, the Follower slowly approaches the Leader towards the end of the drift recovery phase at an approximate rate of 1000 meters per day. During days 76 and 77, the radios on both CubeSats will be turned on to attempt to

acquire a CDGPS lock. Figure 12 shows the 3 components of the CW positions. As soon as the full state feedback controller is activated, all the state errors are driven close to zero.
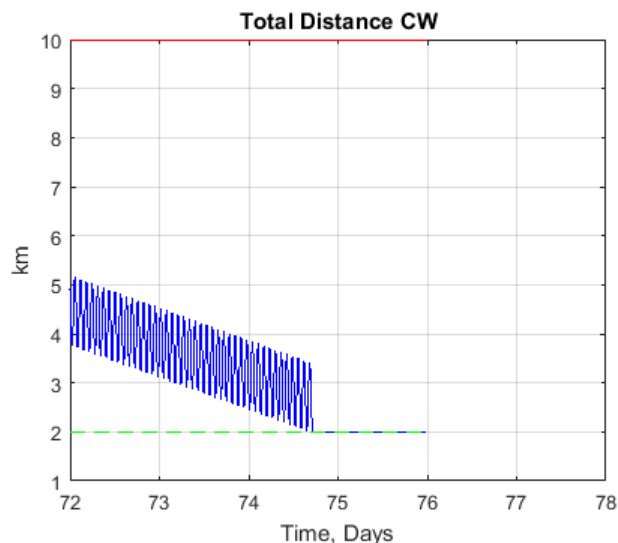
Figure 11. Close Proximity Operation Example: Absolute Rel Position CW frame

Table 7 contains the final CW positions and velocities at the end of the first formation flying phase (20 orbits). Assuming perfect navigation solutions, it is apparent that the LQR controller is fully capable of performing the stationkeeping task. In this baseline example, the ΔV consumed in eliminating the residual differences in the orbital elements from the end of the drift recovery phase to performing precise formation flying for 20 orbits is approximately 3.3 m/s.

Table 7. Example: Final CW States at the end of 1st Formation Flying Phase

| Parameters	Values		
Relative Position, m	[−0.03	−2000.1	0.31]
Relative Velocity, m/s	[0.0005	−0.0063	−0.003]

DOCKING

The docking phase begins when the Follower is within 10 or so meters behind the Leader in the V-bar. Once again, the pair will perform a series of formation flying experiments until the ground station gives the approval to proceed with final docking. Figure 13 illustrates the desired orientations of the Leader of Follower during docking. The Leader is oriented such that its +Z axis is aligned with the local V-bar and the +X axis aligned with the R-bar such that the GPS antenna is pointing away from the Earth. The Follower is rotated 180 deg about the +X axis with respect to the Leader. The magnets inside the docking subsystem are aligned along the +Y axis to generate a larger domain of attraction along the X direction (compared to Y) because CDGPS errors are the greatest in the R-bar direction.

A low bandwidth full-state feedback docking controller about the linear Clohessy-Wiltshire equations[7] (Eq. 12 to 14) was designed to bring the Follower towards the Leader at a few cm/s. There

15
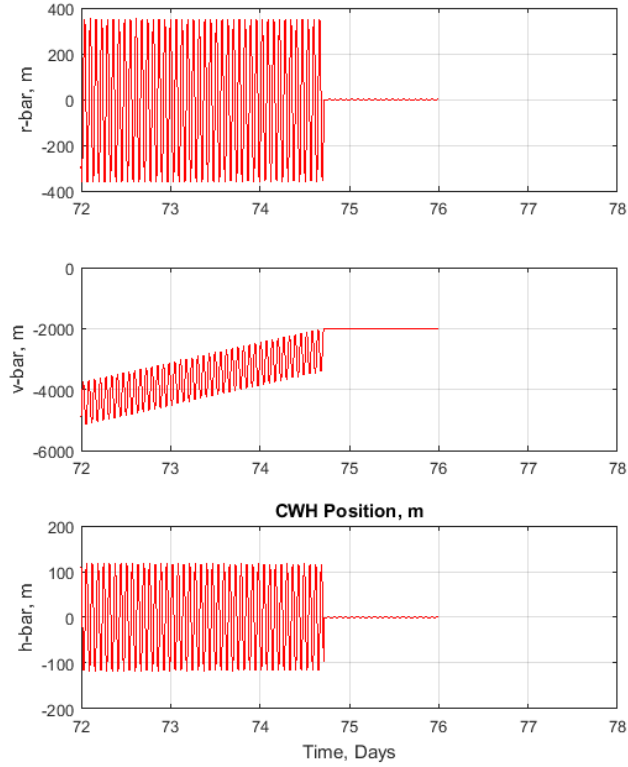
Figure 12. Close Proximity Operation Example: Rel Position CW frame
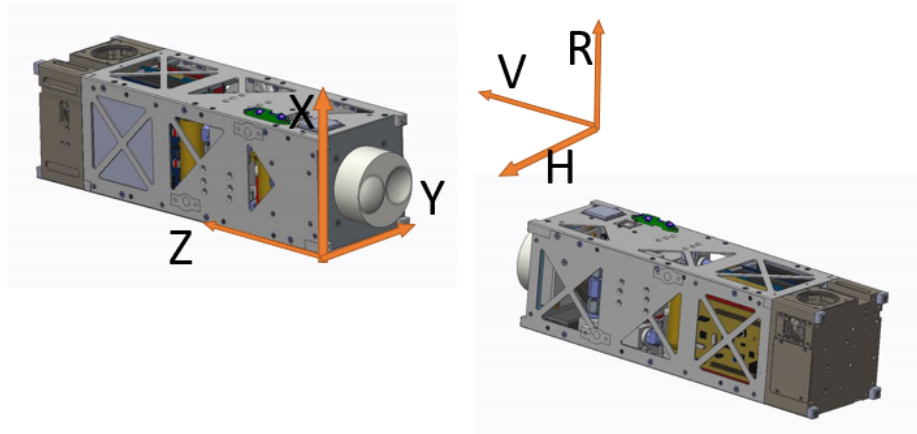
Figure 13. Docking Configuration Schematic

have been numerous studies that explore docking controller strategies.[22–25] A nonlinear phase plane controller also seemed to work well by giving the designer the option to choose the desired coast velocity, position and velocity dead bands etc. in each channel with the magnetic docking subsystem capture volume in mind. The two main objectives are: 1) keep the bandwidth low such that there is

16

roughly an order of magnitude of frequency separation with the attitude loop, 2) make sure that the closed loop poles of the second-order system are well damped with $\zeta > 0.7$. This would ensure that the Follower approaches the magnetic basin of attraction with minimal residual linear velocity.

Since the relative orbital dynamics is linear during the docking phase, both an Extended Kalman Filter (EKF) and a Kalman Filter (KF) are applicable. In the case of KF implementation, the plant dynamics are the linear CW equations. In the case of the EKF, the nonlinear relative equations[19] shown in Eq. 15 to Eq. 19 are used for the plant dynamics (assuming Keplerian orbits). Here x, y, z are the relative separation distances (in-track, cross-track, H-bar) between the Leader and Follower in the Hill frame. μ_x, μ_y, μ_z are the control acceleration inputs for the Follower. r, ω are the radius and orbital angular velocity of the Leader. For small separation distances (<2 km), the two formulations yield nearly identical results.

$$\ddot{x} = 2\omega\dot{z} + \dot{\omega}z + \omega^2 x - \frac{\mu y}{[x^2 + y^2 + (r-z)^2]^{3/2}} + \mu_x \tag{15}$$

$$\ddot{y} = -\frac{\mu y}{[x^2 + y^2 + (r-z)^2]} + \mu_y \tag{16}$$

$$\ddot{z} = -2\omega\dot{z} + \dot{\omega}x + \omega^2 z - \frac{\mu}{r} - \frac{\mu(r-z)}{[x^2 + y^2 + (r-z)^2]^{3/2}} + \mu_z \tag{17}$$

$$\ddot{r} = r\omega^2 - \frac{\mu^2}{r} \tag{18}$$

$$\ddot{\omega} = -\frac{2\dot{r}\omega}{r} \tag{19}$$

Termination conditions in the simulation are: 1) Successful docking, when the offset between the centerlines of the docking interfaces (at an axial separation of 2cm) are within a circle of 1 cm radius. 2) Unsuccessful docking, when the Follower overshoots the Leader or when the magnetic docking subsystem generates large attitude motions in the CubeSats due to excessive misalignment errors between the docking subsystems. Note: collision and contact dynamics are not modeled in the simulation. Table 8 is a comprehensive list of dispersion parameters used for the Monte Carlo simulations. The nominal values are shown in the second column, and the 1σ dispersions are shown in the third column. The magnetic docking mechanism is intended to make the docking process more robust to residual attitude and translation errors.

Figure 14 shows an example of a successful docking trajectory (relative position of the two docking interfaces) in the CW-frame. The Follower starts out at standoff distance of 10 meters in the V-bar direction and slowly moves towards to Leader. Variations in the R-bar and H-bar channels are due to orbital perturbations and system uncertainties. At around T = 880 sec, the Follower enters the magnetic docking subsystem basin of attraction. Thereafter, residual errors in the out-of-plane channels are removed, and the CubeSats dock. Figure 15 shows the final offset between the centerline of the two docking interfaces at a V-bar (axial) separation of 2 cm. It is assume in this analysis that if the relative centerline offset falls within a circle of radius of 1 cm at an axial separation of 2 cm, then successful docking is guaranteed. Figure 16 compares results from a Monte Carlo run showing the final centerline offsets between with and without the magnetic docking subsystem. It is apparent that without the aid of the magnetic docking subsystem (right plot), successful docking is highly unlikely as majority of the dots fall well outside the 1cm unit circle criteria.

Table 8. Dispersions Parameters

| Parameter	Nominal	Uncertainty (1 σ)
Thruster misalignment angle, deg	10-20	5
Thruster mounting offset, m	0	0.0015
Thruster impulse magnitude, %	0	5
CDGPS bias (time varying), m	0	0.02
CDGPS noise, m	0	0.003
Accelometer noise, m/s^2	0	0.002
Accelometer bias, m/s^2	0	2.943×10^{-4}
Gyro drift, rad/s	0	2.67×10^{-5}
Magnetic knockdown factor, %	-20	0
IMU misalignment, deg	0	1.5
Avionic delay, ms	25	0
CG offset, m	0	0.0033
Inertia Iyy, %	0	3
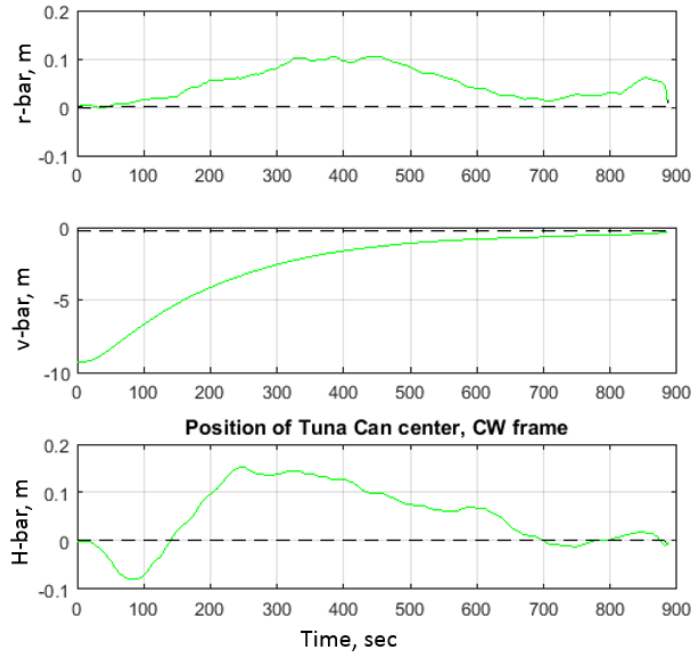
Figure 14. Nominal Successful Docking Trajectory

CONCLUSION

Autonomous rendezvous and docking of two CubeSats in space is a challenging GN&C problem. The algorithm development and simulation results described in this paper provide solid groundwork for a future CubeSat ARD mission. Increased simulation fidelity and STK (Satellite Tool Kit) will be required later in the design cycle. For the baseline mission considered in this paper, approximately 8 m/s of ΔV is required to complete the mission from the beginning of the drift recovery phase to
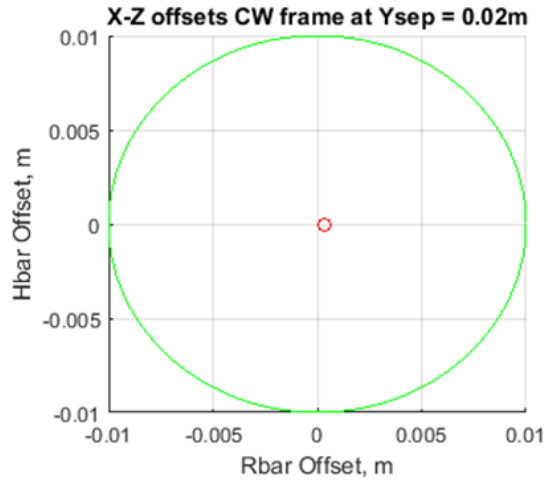
Figure 15. Nominal Successful Docking Example: Final Offset
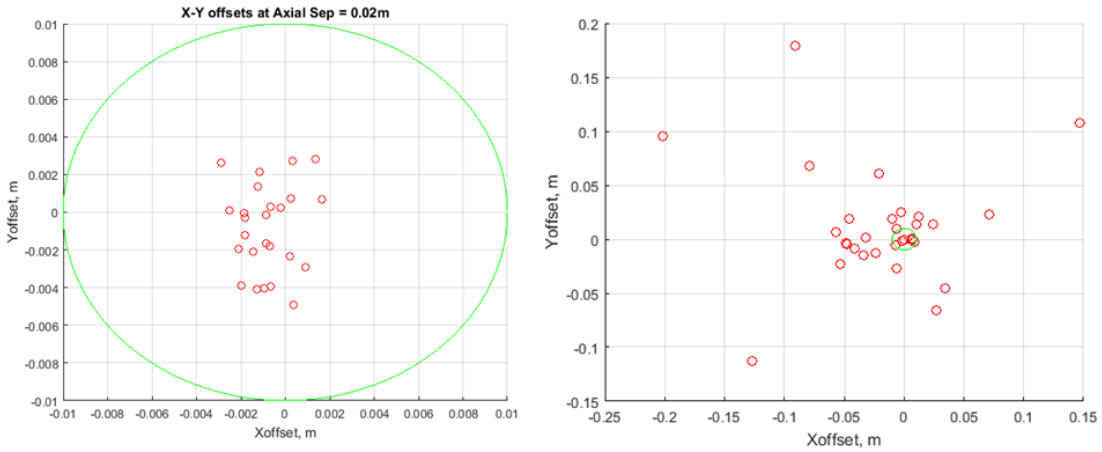
Figure 16. Monte Carlo Results of Final Offset: with and without docking mechanism

final docking, which is well below the total ΔV budgeted for the Follower CubeSat of 16 m/s. This number is certain to increase when inefficiencies of the RCS (Reaction Control System) design such as thrust vector misalignment are considered. In the event of a hardware failure on the Follower, such as a failed thruster or reaction wheel, the dexterity of the GN&C algorithm allows the CubeSats to switch roles and the Leader would be considered as the new Follower. As a concurrent effort, the OAAN team is currently verifying the performance of key system functionalities on the flat floor facility at NASA Langley Research Center.

ACKNOWLEDGEMENTS

REFERENCES

[1] J. Bowen, A. Tsuda, J. Abel, and M. Villa, "CubeSat Proximity Operations Demonstration Mission Update," IEEE, 2015.

[2] M. Nunes, T. Sorenson, and E. Pilger, "On the development of a 6DoF GNC framework for docking multiple small satellites," No. 2015-0868, AIAA SciTech, 2015.

[3] J. Underwood and C. Pellegrino, "Auntonomous Assembly of a Reconfigurable Space Telescope - A CubeSat/Microsatellite Based Technology Demonstrator," No. SSC-VI-5, AIAA/USU Conference on Small Satellites, 2013.

[4] J. Underwood, C. Pellegrino, V. Lappas, C. Bridges, , and J. Baker, "Using CubeSat/micro-satellite technology to demonstrate the Autonomous Assembly of a Reconfigurable Space Telescope," Acta Astronautica, 2015.

[5] J. Griesbach, J. Westphal, C. Roscoe, and et, "Proximity Operations Nano-Satellite Flight Demonstration Rendezvous Proximity Operations Design and Trady Study Results,"

[6] J. Pei and L. Murchison, "Ground Demonstration on the Autonomous Docking of Two 3U CubeSats Using a Novel Permanent-Magnet Docking Mechanism," No. 2017-0849, AIAA, 2017.

[7] W. Clohessy and R. Wiltshire, "Terminal Guidance System for Satellite Rendezvous," *Journal of the Aerospace Sciences*, Vol. 27, No. 9, 1960, pp. 653–658.

[8] Rock Seven Location Technology, *RockBlock DataSheet*, 2016.

[9] G. Bonin and N. Roth, "CanX-4 and CanX-5 Precision Formation Flight: Mission Accomplished," No. SSC15-I-4, Small Sat Conference, 2015.

[10] J. Newman, "Drift Recovery and Station Keeping Results for the Historic CanX-4 and CanX-5 Formation Flying Mission," No. SSC15-VIII-1, Small Sat Conference, 2015.

[11] SwiftNav, *Piksi DataSheet*, June 2013.

[12] J. Pei, L. Murchison, , and et, "Autonomous Rendezvous and Docking of Two 3U CubeSats Using a Novel Permanent-Magnet Docking Mechanism," No. 2016-1465, AIAA, 2016.

[13] S. Mohiuddin and M. Psiaki, "High-Altitude Satellite Relative Navigation Using Carrier-Phase Differential Global Positioning System Techniques," *Journal of Spacecraft and Rockets*, Vol. 30, Sept-Oct 2007.

[14] S. Leung and O. Montebrucki, "Real-Time Navigation of Formation-Flying Spacecraft using Global-Positioning-System Measurements," *Journal of Guidance, Control, and Dynamics*, Vol. 28, Mar-Apr 2005.

[15] Blue Canyon Technologies, *XACT DataSheet*, Feb 2015.

[16] S. M, *Spacecraft Dynamics and Control*. Cambridge University Press, fifth ed., 2006.

[17] C. Roithmayr, "Contribution of Spherical Harmonics to Magnetic and Gravitational Fields," No. NASA TM-2004-213007, NASA, 2004.

[18] D. Vallado and M. Wayne, *Fundamentals of Astrodynamics and Applications*. McGraw-Hill, 2001.

[19] H. Schaub and J. Junkins, *Analytical Mechanics of Space Systems*. AIAA, 2003.

[20] J. Crassidis, *State Estimation of Dynamical Systems*. 2010.

[21] D. Gaylor and B. Barbee, "Algorithms for Safe Spacecraft Proximity Operations," No. 2007-107, AAS, 2007.

[22] P. Singla, K. Subbarao, , and J. Junkin, "Adaptive Output Feedback Control for Spacecraft Rendezvous and Docking Under Measurement Uncertainty," *Journal of Guidance, Control, and Dynamics*, Vol. 29, July-August 2006.

[23] C. Kluever, "Feeback Control for Spacecraft Rendezvous and Docking," *Journal of Guidance, Control, and Dynamics*, Vol. 22, July-August 1999.

[24] C. Tournes, Y. Shtessel, and D. Foreman, *Sliding Mode Control*. InTech, 2011.

[25] S. Cairano, H. Park, and I. Kolmanovsky, "Model Predictive Control Approach for Guidance of Spacecraft Rendezvous and Proximity Maneuvering," *International Journal of Robust and Nonlinear Control*, Vol. 22, May 2012, pp. 1398–1427.